POLITECNICO
MILANO 1863

# *Spacecraft Attitude Dynamics and Control*

**Department of Aerospace**
**Science and Technology**

---

**12U cubesat:**
**Detumbling, Slew manoeuvre and Earth pointing**

Bardazzi, Niccolò PC: 10800456, MN: 963039

MSc in Space Engineering - AY 2020/2021

# Contents

Chapter 1

# Introduction

The aim of the following project is to study the attitude dynamics and the control system of a 12U cubesat placed in a Low Earth Orbit. The spacecraft is injected with a high angular velocity hence the goal to slow it down firstly and then to stabilize its motion during its lifetime.

It has been taken as mission an Earth observation one for science or commercial purposes.

The phases to be dealt with are:

- **Detumbling phase**
- **Slew manoeuvre**
- **Earth pointing**

## 1.1 Orbit

Orbital elements displayed in the table below are taken from a real satellite whose orbit is a polar orbit.

| **Orbital parameters** | |
|---|---|
| **a**[**km**] | 7197 |
| **e** | 0.0002084 |
| **i**[°] | 98.7116 |
| $\omega$[°] | 271.7368 |
| $\mathbf{\Omega}$[°] | 95.6830 |

## 1.2 Structure

The satellite is a CubeSat composed of 12 units. The weight of the satellite has been estimated considering 3 kg per unit for a total weight of 36 kg. The dimensions of the external structure are hence 300mm x 200mm x 200mm while inertia matrix is:

$$I = \begin{bmatrix} 11.25 & 0 & 0 \\ 0 & 18.25 & 0 \\ 0 & 0 & 18.72 \end{bmatrix} \tag{1.1}$$

Chapter 2

# Sensors

## 2.1 Noise

Sensors' measurements are affected to white noise which has been modelled with a rotation around the exact measure with a Euler angles parametrization matrix:

$$m_k = v_k \cdot A_{eps} \tag{2.1}$$

where $m_k$ is the noisy measure, $v_k$ is the exact value and $A_{eps}$:

$$A_{eps} = \begin{bmatrix} cos(\psi)cos(\theta) & cos(\psi)sin(\theta)sin(\phi) + sin(\psi)cos(\phi) & -cos(\psi)sin(\theta)cos(\phi) + sin(\psi)sin(\phi) \\ -sin(\psi)cos(\theta) & -sin(\psi)sin(\theta)sin(\phi) + cos(\psi)cos(\phi) & sin(\psi)sin(\theta)cos(\phi) + cos(\psi)sin(\phi) \\ sin(\theta) & -cos(\theta)sin(\phi) & cos(\theta)cos(\phi) \end{bmatrix} \tag{2.2}$$

$\psi, \theta, \phi$ are random numbers generated by Simulink according to the covariance of the single sensor reported in its own catalogue.

## 2.2 Sun sensor

Limitations of this kind of sensors are solar eclipses (which has been implemented in SRP model) that can make the sensor failing for a part of the orbit. For this reason 6 analog sun sensors have been mounted over the six faces of the structure. The accuracy of this kind of sensors is very high hence they have been used for the attitude determination, when possible. Their output is a current and its internal dynamics has been modelled with a cosine law.

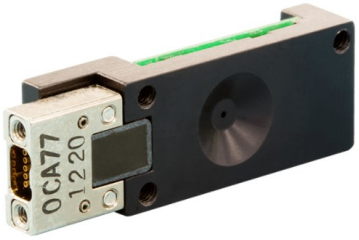


Figure 2.1: Sun sensors

| Parameter | Characteristics |
|---|---|
| Pointing accuracy | $< 0.100°$ |
| Update rate | 5 Hz |
| FOV | 120° |
| Dimensions | 34 x 32 x 20 mm |
| Manufacturer | CubeSatShop |

Table 2.1: Data from catalogue

## 2.3 Earth Horizon

Earth horizon sensors use thermopile detectors to detect nadir direction. They work in infrared spectrum and usually have 4 termopiles: 1 with a higher FOV but less accuracy while the other 3 are more accurate and are oriented respectively to space, limb and Earth (MIT). This sensor will be used during the eclipse phase as the only measurement available for the Kalman Filter. The choice to couple an Earth Horizon sensor with a Sun sensor is due to the orbit requirement. Indeed the orbit is almost a sun-synchronous orbit thus the two measurements should never be aligned between them, this means that the attitude determination is always possible if the two sensors are working.

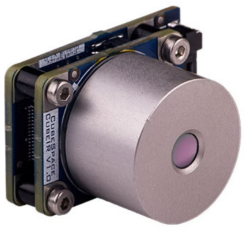

Figure 2.2: Earth horizon sensor

| Parameter | Characteristics |
|---|---|
| Pointing accuracy | 0.250° |
| Fine FOV | $> 7°$ |
| Coarse FOV | 60° |
| Update rate | 2 Hz |
| Dimensions | 43.3 x 31.8 x 20.7 mm |
| Manifacturer | SatCatalog |

Table 2.2: Data from catalogue

Chapter 3

# Actuators

Actuators used for the detumbling phase are 4 variable gas jets.
During the slew manoeuvre and Earth pointing phase it has been used reaction wheels for 2 reasons:

- provide a much more accurate torque action than gas jets in the attitude
- need no fuel thus the mission can last longer

## 3.1 Variable gas jets

Four cold gas thrusters have been disposed according to a pyramid configuration. Since it is not known a priori the torque required, the pyramid has a square base for an equal partitioning 3.1.

$$A_t = \begin{bmatrix} \blacksquare & 1 & -1 & -1 \\ -1 & 1 & 1 & -1 \\ 1 & -1 & 1 & -1 \end{bmatrix} \tag{3.1}$$

This pyramid matrix can be used to simplify computations: instead of performing for each couple of thrusters $T_{couple} = (r_1 - r_2) \wedge F$ it is possible to build a configuration matrix $[\hat{R}]$ such that $T_{tot} = [\hat{R}]F$.

$$[\hat{R}] = \begin{bmatrix} l \cdot sin(\alpha) & 0 & 0 \\ 0 & l \cdot cos(\alpha) & 0 \\ 0 & 0 & x \cdot sin(\alpha) - x \cdot cos(\alpha) \end{bmatrix} \begin{bmatrix} 1 & 1 & -1 & -1 \\ -1 & 1 & 1 & -1 \\ 1 & -1 & 1 & -1 \end{bmatrix} \tag{3.2}$$

Assumption:

- actuators are not with null resultant, however it is considered to be negligible for the aim of the project;
- the fuel consumption can modify the inertia matrix as well as the weight of the satellite, this is not taken into account for the dynamics.

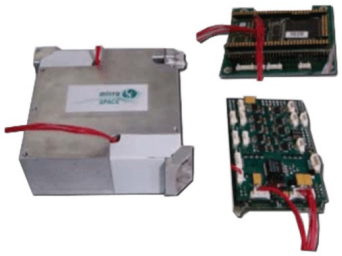

Figure 3.1: Cubesatshop micropropulsion

| Parameter | Characteristics |
|---|---|
| Nominal thrust | 100 $\mu N$ - 10 $mN$ |
| Specific Impulse | 50 - 100 $s$ |
| Raise time | 10 $ms$ |
| Fall time | 50 $ms$ |
| Delay time | 5 $ms$ |
| Raise time | 10 $ms$ |
| Manifacturer | MicroSpace |

Table 3.1: Data from catalogue

## 3.2 Reaction wheels

Reaction wheels are momentum exchange devices that have been used for a fine regulation of the angular velocities. They have been disposed along three axis and diagonal according to Equation 3.3. This kind of configuration is very useful in the case one of the reaction wheels stops working.

$$A_{rw} = \begin{bmatrix} 1 & 0 & 0 & \frac{1}{\sqrt{3}} \\ 0 & 1 & 0 & \frac{1}{\sqrt{3}} \\ 0 & 0 & 1 & \frac{1}{\sqrt{3}} \end{bmatrix} \tag{3.3}$$

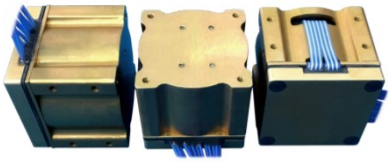

Figure 3.2: Cubesatshop reaction wheels

| Parameter | Characteristics |
|---|---|
| Maximum momentum | 2.3 $mN \cdot m$ |
| Momentum storage | 30 $mN \cdot m \cdot s$ |
| Dimensions | 57 x 57 x 31.5 $mm$ |
| Manifacturer | CubeSpace |

Table 3.2: Data from catalogue

Chapter 4

# Environmental disturbances

Environmental disturbances actually should be known by sensors, therefore it should be the output of a black box which is fed to sensors. However they can also be modelled with a sufficient high accuracy like what has been done in this project. This kind of disturbances acts as an additional torque which changes the dynamic of the problem according to Euler equations:

$$\begin{cases} \dot{\omega}_x = \frac{I_y - I_z}{I_x}\omega_y\omega_z + \frac{M_x}{I_x} \\ \dot{\omega}_y = \frac{I_z - I_x}{I_y}\omega_z\omega_x + \frac{M_y}{I_y} \\ \dot{\omega}_z = \frac{I_x - I_y}{I_z}\omega_x\omega_y + \frac{M_z}{I_z} \end{cases} \tag{4.1}$$

Assumption:

- the motion of the spacecraft is a rigid body motion. Since this satellite is a compact and small one this is a good assumption;
- inertia matrix is diagonal, there are no centrifugal terms.

## 4.1 Gravity gradient

Gravity gradient is a perturbation due to the different distance between the attraction body (taken as a mass concentrated point) and all the points of the satellite. This disturbance can be relevant when the spacecraft is a big one or when the orientation of even a small spacecraft is such that the two edges of the body are not at the same distance with respect to Earth (e.g. during the slew manoeuvre).
Torque applied in 4.1 is:

$$\mathbf{T}_{gg} = \frac{3\mu}{r^3}\left[c_2c_3\left(I_z - I_y\right) \quad c_1c_3\left(I_z - I_x\right) \quad c_1c_2\left(I_x - I_y\right)\right]^T \tag{4.2}$$

where $c = [c_1 \quad c_2 \quad c_3]^T$ has been computed as:

$$c = A_{BL}[1 \quad 0 \quad 0]^T \tag{4.3}$$

## 4.2 Aerodynamic drag

Aerodynamic drag is modelled as if the spacecraft is moving in a fluid according to the equation:

$$\mathbf{T}_{\mathrm{AD}} = -\frac{1}{2}\rho C_D v_{rel}^2 \sum_{i=1}^{n} r_i \times \left( n_{si} \cdot \frac{v_{rel}}{\|v_{rel}\|} \right) \frac{v_{rel}}{\|v_{rel}\|} S_i \tag{4.4}$$

Note that this equation is valid until the density can be considered as a continuous function. Nevertheless it is not always true in the space environment, fluid's density has been interpolated from the Table 4.1 (Biggs) which provides a good approximation. It has also been considered that all the surfaces with a negative drag force are not taken into account in the sum.

| altit. (km) | 10 | 20 | 30 | 40 | 50 | 60 | 70 | 80 | 90 | 100 |
|---|---|---|---|---|---|---|---|---|---|---|
| density (g/cm$^3$) | 4,02e-04 | 8,34e-05 | 1,57e-05 | 3,18e-06 | 8,37e-07 | 2,33e-07 | 5,86e-08 | 1,40e-08 | 2,99e-09 | 5,17e-10 |
| altit. (km) | 110 | 120 | 130 | 140 | 150 | 160 | 170 | 180 | 190 | 200 |
| density (g/cm$^3$) | 8,42e-11 | 1,84e-11 | 7,36e-12 | 3,78e-12 | 2,19e-12 | 1,37e-12 | 9,00e-13 | 6,15e-13 | 4,32e-13 | 3,10e-13 |
| altit. (km) | 210 | 220 | 230 | 240 | 250 | 260 | 270 | 280 | 290 | 300 |
| density (g/cm$^3$) | 2,27e-13 | 1,68e-13 | 1,26e-13 | 9,58e-14 | 7,35e-14 | 5,68e-14 | 4,43e-14 | 3,48e-14 | 2,75e-14 | 2,18e-14 |
| altit. (km) | 310 | 320 | 330 | 340 | 350 | 360 | 370 | 380 | 390 | 400 |
| density (g/cm$^3$) | 1,74e-14 | 1,40e-14 | 1,13e-14 | 9,10e-15 | 7,39e-15 | 6,02e-15 | 4,92e-15 | 4,03e-15 | 3,31e-15 | 2,72e-15 |
| altit. (km) | 410 | 420 | 430 | 440 | 450 | 460 | 470 | 480 | 490 | 500 |
| density (g/cm$^3$) | 2,25e-15 | 1,86e-15 | 1,54e-15 | 1,28e-15 | 1,07e-15 | 8,89e-16 | 7,43e-16 | 6,22e-16 | 5,22e-16 | 4,39e-16 |
| altit. (km) | 510 | 520 | 530 | 540 | 550 | 560 | 570 | 580 | 590 | 600 |
| density (g/cm$^3$) | 3,71e-16 | 3,13e-16 | 2,66e-16 | 2,26e-16 | 1,93e-16 | 1,65e-16 | 1,41e-16 | 1,22e-16 | 1,05e-16 | 9,14e-17 |
| altit. (km) | 610 | 620 | 630 | 640 | 650 | 660 | 670 | 680 | 690 | 700 |
| density (g/cm$^3$) | 7,96e-17 | 6,97e-17 | 6,12e-17 | 5,41e-17 | 4,79e-17 | 4,27e-17 | 3,82e-17 | 3,44e-17 | 3,10e-17 | 2,82e-17 |
| altit. (km) | 710 | 720 | 730 | 740 | 750 | 760 | 770 | 780 | 790 | 800 |
| density (g/cm$^3$) | 2,57e-17 | 2,35e-17 | 2,16e-17 | 1,99e-17 | 1,84e-17 | 1,71e-17 | 1,59e-17 | 1,49e-17 | 1,39e-17 | 1,31e-17 |
| altit. (km) | 810 | 820 | 830 | 840 | 850 | 860 | 870 | 880 | 890 | 900 |
| density (g/cm$^3$) | 1,23e-17 | 1,16e-17 | 1,10e-17 | 1,04e-17 | 9,86e-18 | 9,37e-18 | 8,91e-18 | 8,48e-18 | 8,09e-18 | 7,72e-18 |
| altit. (km) | 910 | 920 | 930 | 940 | 950 | 960 | 970 | 980 | 990 | 1000 |
| density (g/cm$^3$) | 7,37e-18 | 7,04e-18 | 6,74e-18 | 6,45e-18 | 6,18e-18 | 5,92e-18 | 5,68e-18 | 5,44e-18 | 5,22e-18 | 5,02e-18 |

Table 4.1: Air drag data

Assumption:

- the torque has not been computed by the integral on the surface of the infinitesimal drag force but with the centre of mass of each surface;

- the Earth is considered a sphere (for the altitude) and its atmosphere has constant value of density even if there could be seasonal and daily variations.

## 4.3 Magnetic field

Magnetic field model on the on board computer is the one computed with no approximations from the $13^{th}$ order Legendre polynomial. Its coefficients were achieved easily by Gauss orthonormalization since it is a recursive model. It has been decided to use such an accurate model since the spacecraft is on a LEO orbit (altitude 825 km) therefore the dipole model is not a reliable model. The magnitude of the magnetic field for the chosen orbit has been displayed in Figure 4.1 .

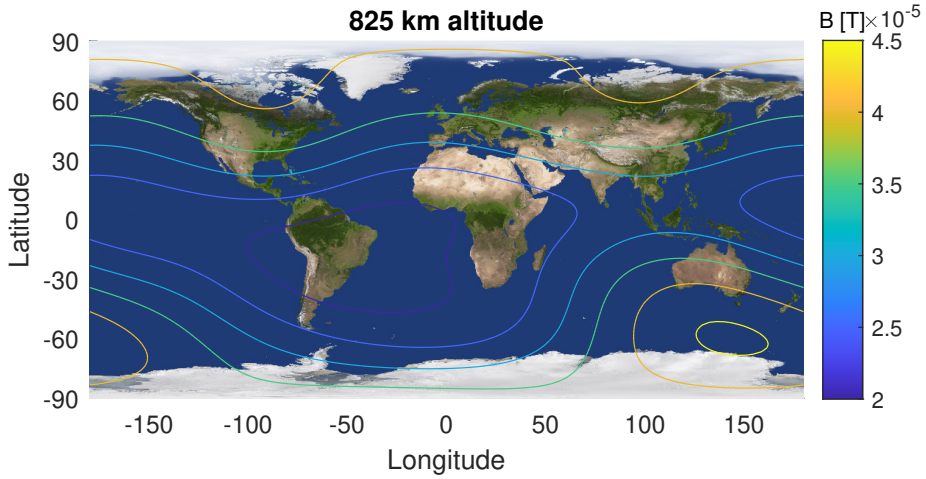


Figure 4.1: Magnitude of magnetic field at 825 km altitude

All the $g_n^m$, $h_n^m$ coefficients of Equation 4.5 for the magnetic field have been taken from (3).

$$V(r,\theta,\phi) = a\sum_{n=1}^{k}\left(\frac{a}{r}\right)^{n+1}\sum_{m=0}^{n}\left(g_n^m\cos m\phi + h_n^m\sin m\phi\right)P_n^m(\theta) \tag{4.5}$$

## 4.4 Solar Radiation Pressure

SRP has been modelled as a force which acts on solar panels and has different intensity according to specular and diffuse reflection coefficients. Solar panels of the satellite has the following properties:

| | |
|---|---|
| Dimensions | 300mm x 200mm |
| $\rho_{MBd}$ | 0.1 |
| $\rho_{MBs}$ | 0.5 |
| $\rho_{SPd}$ | 0.1 |
| $\rho_{SPs}$ | 0.8 |

The subscript $MB$ stands for main body, $SP$ solar panels, $d$ diffusive coefficient, $s$ specular coefficient.
SRP has been modelled like a force 4.6 that acts on every surfaces and whether $\hat{S}\cdot\hat{n}_s$ is negative the contribute has not been considered.

$$\underline{F} = -PA\left(\hat{S}\cdot\hat{n}_s\right)\left[\left(1-\rho_s\right)\hat{S} + \left(2\rho_s\left(\hat{S}\cdot\hat{n}_s\right) + \frac{2}{3}\rho_d\right)\hat{n}_s\right] \tag{4.6}$$

It has also been considered the case of the solar eclipse with a cylindrical shadow model, when Equation 4.7 is satisfied the satellite is not in eclipse.

$$\underline{S}_N \cdot \underline{r}_N > -\sqrt{|\underline{r}_N|^2 - R_E^2} \tag{4.7}$$

## 4.5 Ignored contributes

Other perturbations that are not taken into account are:

- Earth oblateness (J2);
- Moon perturbations (third body).

Actually since the orbit is a LEO the third body perturbations are not so relevant but J2 could lead to errors with respect to a real satellite if the model would have been propagated for a big time span.

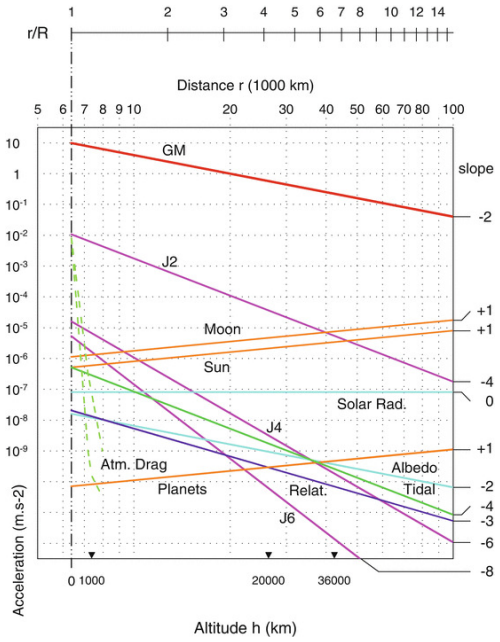

Chapter 5

# Detumbling

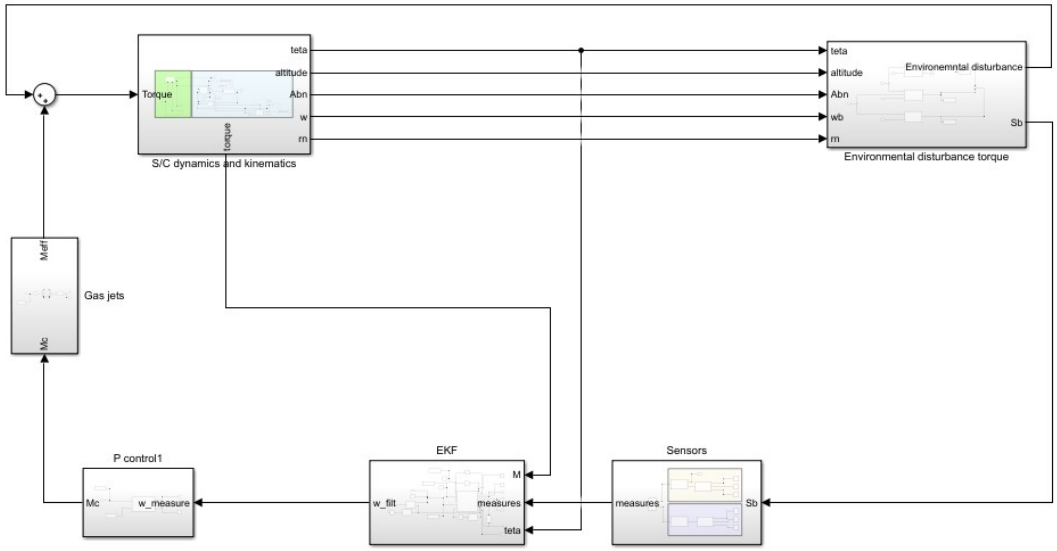


Figure 5.1: Detumbling phase Simulink model

In order to start the simulation initial condition spacecraft orientation must be chosen:

$$w_0 = \begin{bmatrix} 0.22 \\ 0.26 \\ 0.22 \end{bmatrix} \quad \text{and} \quad A_{B/N} = \begin{bmatrix} 0.5335 & 0.808 & 0.25 \\ -0.808 & 0.3995 & 0.433 \\ 0.25 & -0.433 & 0.866 \end{bmatrix} \tag{5.1}$$

They are considered unknown from spacecraft point of view, for this reason attitude determination is necessary as the first step of detumbling. After an appropriate time (2 seconds has been considered as enough) the Kalman Filter will be switched on starting the estimation with the data from the determination done before.

## 5.1 Thrusters control

Regarding variable gas jets, it has been computed firstly the maximum torque available according to 5.2.

$$T_{max} = \begin{bmatrix} T_{max_x} & 0 & 0 \\ 0 & T_{max_y} & 0 \\ 0 & 0 & T_{max_z} \end{bmatrix} \tag{5.2}$$

where:

- $T_{max_x} = 2l \cdot F_{max} cos(\alpha)$
- $T_{max_y} = 2l \cdot F_{max} sin(\alpha)$
- $T_{max_z} = 2(x \cdot F_{max} cos(\alpha) - x \cdot F_{max} sin(\alpha))$

(It was possible also to compute it from the configuration matrix $[\hat{R}]$ with a vector of forces $F_{max}$ two by two)

The same procedure has been repeated for the minimum available torque. For control torque it has been used a proportional control:

$$M = -k \cdot sign(\omega) \tag{5.3}$$

k is the proportional coefficient which has been tuned to 0.01 satisfying time and fuel requirements. This kind of control makes the system asymptotically stable according to Lyapunov's stability theorem. The logic implemented is the one that involves switching on thrusters whose providing torque slows down the maximum angular velocity of that instant. Thrusters are kept on until $|M_{req}| > T_{min}$.

## 5.2 Results

As it is possible to notice from Figure 5.2 the control action takes $\underline{\omega}$ to zero with less than 200 s. On the upper side it has been displayed the angular velocities coming from kinematic while lower side the angular velocities from the Kalman observer.

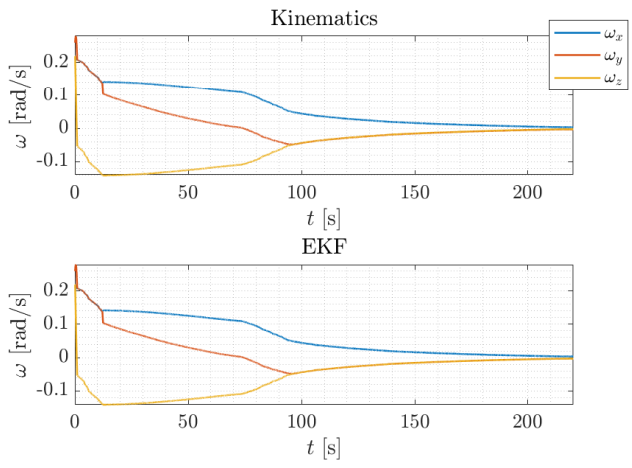


Figure 5.2: Angular velocities in body frame

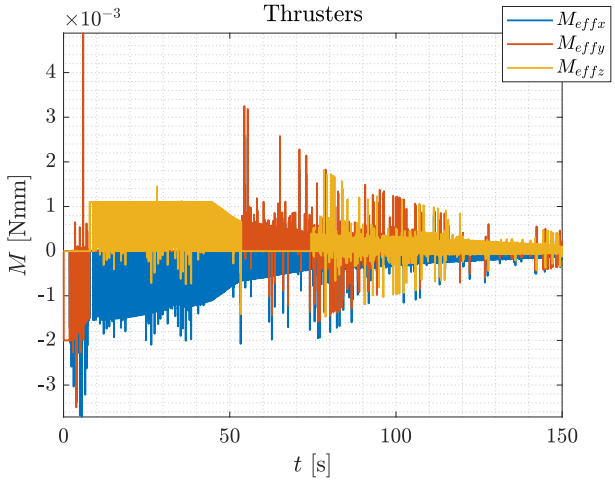


Figure 5.3: Effective torque of thrusters

In the Figure 5.3 it has been displayed which is the torque provided to the spacecraft by thrusters before turning them off.

In order to get the force of each single thruster which are coupled for every control action (Figure 5.4), firstly it has been computed the configuration matrix $[\hat{R}]$ according to section 3.1, then since the force provided must always be positive an additional term proportional to the null vector of $[\hat{R}]$, $\gamma w$, has been added ($w$ is the null vector of $[\hat{R}]$). Hence:

$$\underline{F} = \hat{R}^* \underline{M_c} + \gamma \tag{5.4}$$

where:

$$\gamma = max_{i=1,..,N}([\hat{R}]^* \underline{M_c})_i / w_i \quad \text{and} \quad w = \begin{bmatrix} 0.5 \\ 0.5 \\ 0.5 \\ 0.5 \end{bmatrix} \tag{5.5}$$

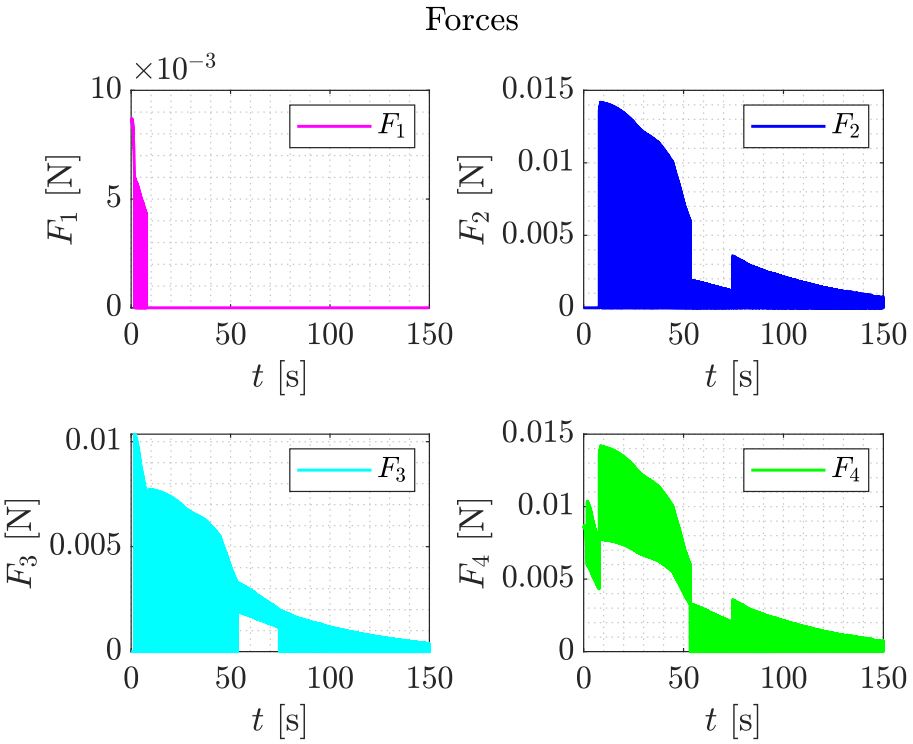


Figure 5.4: Thrusters' respective force applied

# Chapter 6

# Slew manoeuvre

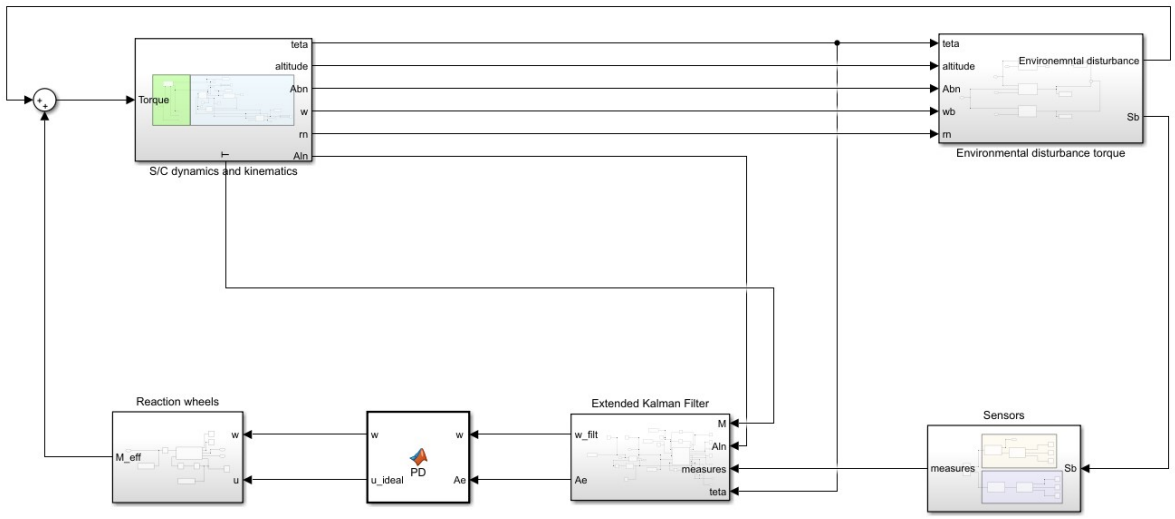


Figure 6.1: Slew manoeuvre Simulink model

The aim of the slew manoeuvre is to perform a rest to rest manoeuvre capable of reaching the desired attitude. In this case the desired orientation is moving hence the only difference between the slew manoeuvre and the earth pointing phase are the PD gains and the observer settings which has been tuned according to the most convenient response and the less noisy observation respectively.

## 6.1 Reaction wheels control

Control action has been achieved with a Proportional Derivative controller (Equation 6.1)

$$\underline{u_c} = -k_p \cdot \underline{\alpha_e} - k_d \cdot \underline{\omega_e} \tag{6.1}$$

where: $k_p = 0.005$, $k_d = 0.12$, $\underline{\alpha_e}$ is the error with respect to the desired attitude:

$$\underline{\alpha_e} = \begin{bmatrix} A_{eps}(3,2) \\ A_{eps}(1,3) \\ A_{eps}(2,1) \end{bmatrix} \qquad A_{eps} = (A_e^T - A_e) \quad \text{and} \quad A_e = A_{B/N} A_{ln} \tag{6.2}$$

and $\underline{\omega_e}$ is the relative error with respect to the moving frame:

$$\underline{\omega_e} = \underline{\omega} - A_e \underline{\omega_d} \qquad \text{but} \qquad \underline{\omega_d} = \underline{0} \tag{6.3}$$

## 6.2 Results

What we expect from a slew manoeuvre is an alignment with the desired attitude from the initial random orientation inherited from the detumbling phase. This is exactly what has been displayed in Figure 6.2. The match has been reached within 80 s from very far initial conditions.

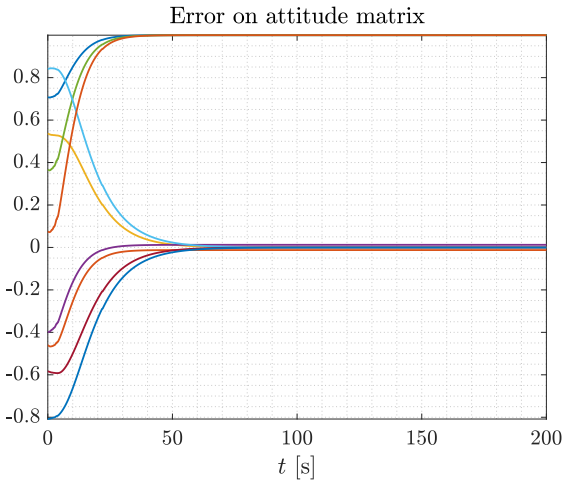


Figure 6.2: Error on orientation

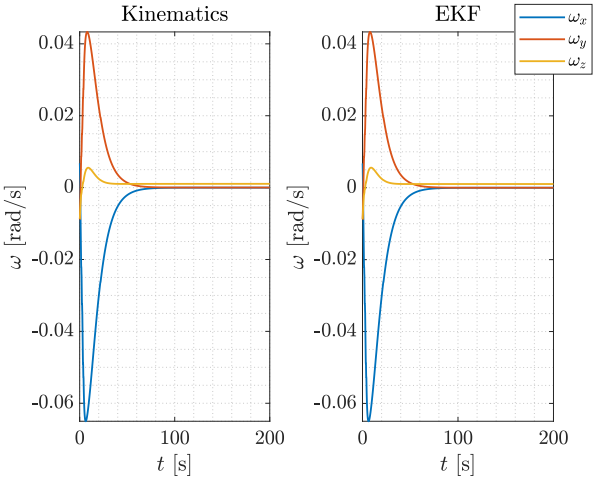


Figure 6.3: Angular velocity during the manoeuvre

Reaction wheels has been kept far below the saturation point which was 30 mN·m·s, as displayed in Figure 6.4

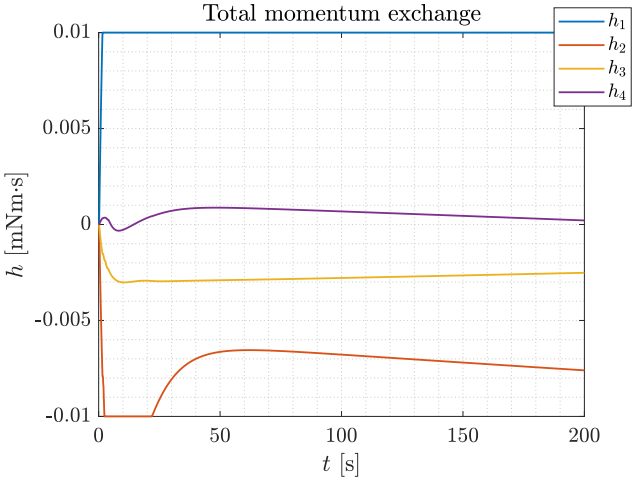


Figure 6.4: Total momentum exchanged with reaction wheels

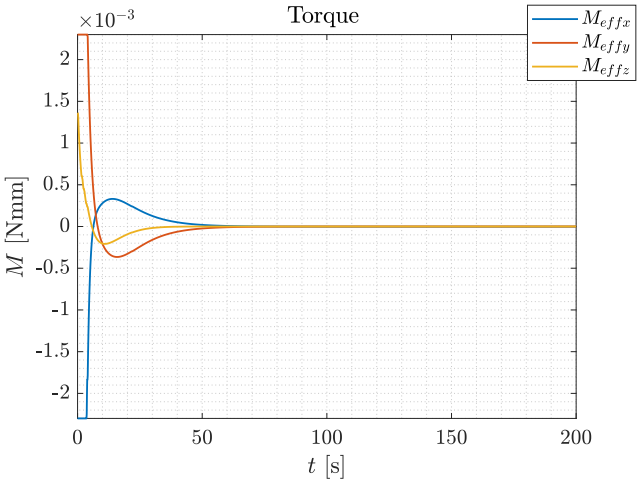


Figure 6.5: Torque provided during the manoeuvre

All the perturbation have been studied also in order to understand which were the most influencing during the Earth pointing phase and as it is possible to see from Figure 6.6, gravity gradient has its maximum in the middle of the manoeuvre but then it goes to zero, as we expected.

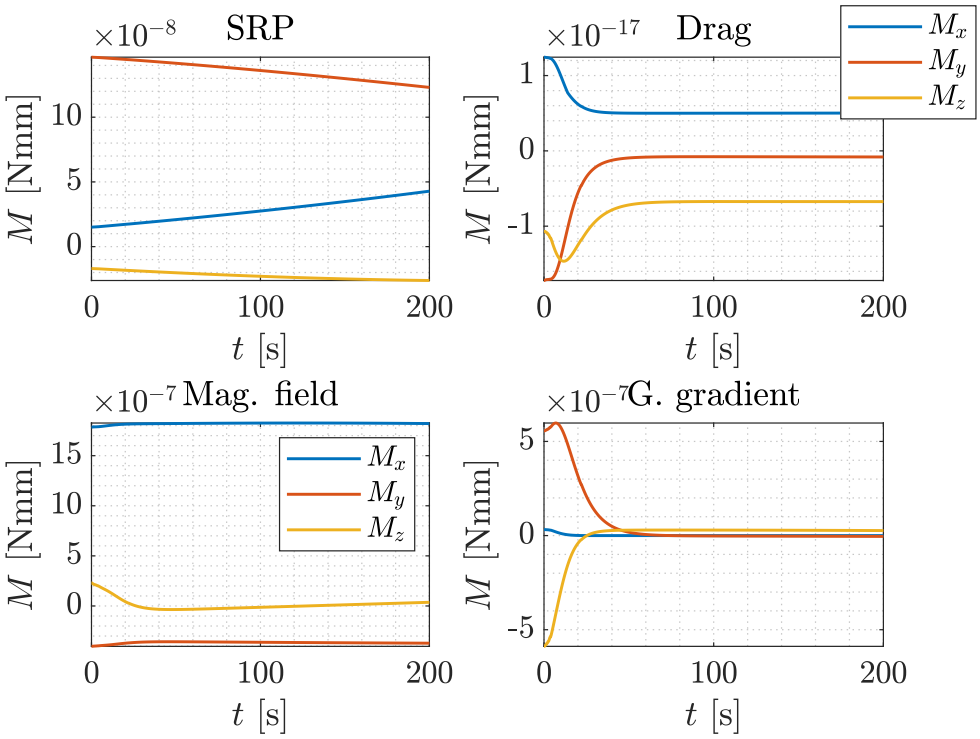


Figure 6.6: Perturbations' torques

Chapter 7

# Earth pointing

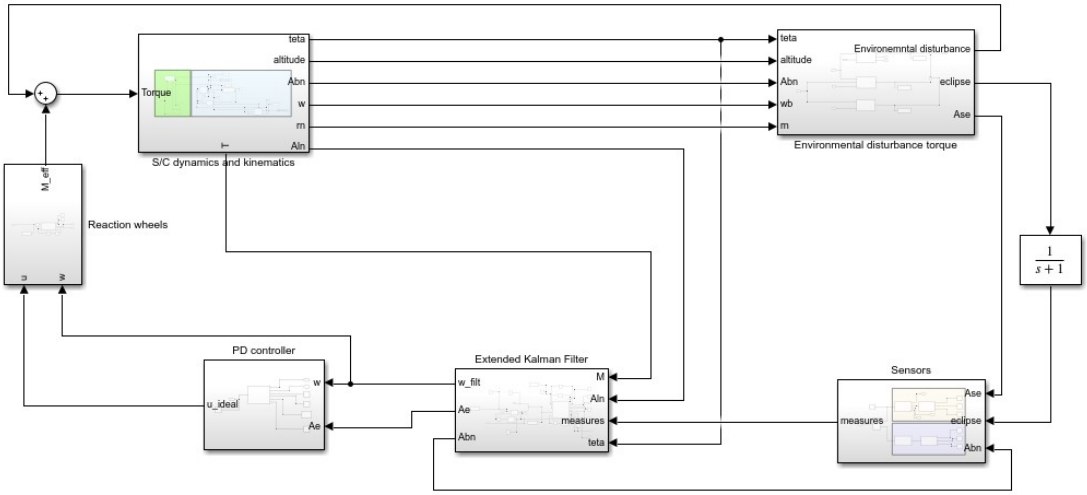


Figure 7.1: Earth pointing Simulink model

For the Earth pointing phase it is required that:

$$\omega_z = \omega_E \quad \text{and} \quad \omega_E = \frac{T}{\sqrt{\frac{\mu}{a^3}}} \simeq 0.001034 \quad [rad/s] \tag{7.1}$$

Therefore:

$$\underline{\omega_d} = \begin{bmatrix} 0 \\ 0 \\ \omega_E \end{bmatrix} \tag{7.2}$$

While gains now are $k_p = [0.1\ 0.1\ 1.1]$ and $k_d = [0.01\ 0.01\ 0.007]$.

## 7.1 Attitude determination

Attitude determination, as previously said, has been used as initial condition for attitude estimation. This also means that until attitude determination hasn't given an output, the estimation cannot starts.
TRIAD method is the most straightforward method to be used thanks to its robustness and low computational cost:

- TRIAD method cannot have singularities (robustness);
- computations are only cross products and matrix multiplication, Equation 7.3 and Equation 7.4 (low cost).

$$\begin{aligned} s_1 &= p \\ s_2 &= \tfrac{p\times q}{|p\times q|} \\ s_3 &= p \times s_2 \\ v_1 &= a \\ v_2 &= \tfrac{a\times b}{|a\times b|} \\ v_3 &= a \times v_2 \\ S &= \begin{bmatrix} s_1 & s_2 & s_3 \end{bmatrix} \\ V &= \begin{bmatrix} v_1 & v_2 & v_3 \end{bmatrix} \end{aligned} \tag{7.3}$$

$$A_{B/N} = SV^{-1} = SV^T \tag{7.4}$$

Nevertheless its strength, no attitude determination methods can work just with 1 measurements, hence it has been expected that the satellite will start detumbling with Sun lights.

## 7.2 Extended Kalman Filter

Attitude estimation is the most reliable way to know attitude characteristics of the spacecraft during the whole orbit. The estimation algorithm works with even 1 measurement available and for this is reason it has been implemented since during the eclipse phase all the sun sensors stop working.
Estimation algorithm is an Extended Kalman Filter (EKF) which is a non-linear observer (because of the non-linear dynamics described by Euler's equations) which plays the key role of changing the observers' gain in order to minimize the covariance matrix. Instead of using its continuous version, it has been linearized since we are expecting to work near the equilibrium point.
EKF algorithm is:

$$\begin{aligned} \hat{\boldsymbol{x}}_{k|k-1} &= f\left(\hat{\boldsymbol{x}}_{k-1|k-1}, \boldsymbol{u}_k\right) \\ \boldsymbol{P}_{k|k-1} &= \boldsymbol{F}_k \boldsymbol{P}_{k-1|k-1} \boldsymbol{F}_k^\top + \boldsymbol{Q}_k \\ \tilde{\boldsymbol{y}}_k &= \boldsymbol{z}_k - h\left(\hat{\boldsymbol{x}}_{k|k-1}\right) \\ \boldsymbol{S}_k &= \boldsymbol{H}_k \boldsymbol{P}_{k|k-1} \boldsymbol{H}_k^\top + \boldsymbol{R}_k \\ \boldsymbol{K}_k &= \boldsymbol{P}_{k|k-1} \boldsymbol{H}_k^\top \boldsymbol{S}_k^{-1} \\ \hat{\boldsymbol{x}}_{k|k} &= \hat{\boldsymbol{x}}_{k|k-1} + \boldsymbol{K}_k \tilde{\boldsymbol{y}}_k \\ \boldsymbol{P}_{k|k} &= \left(\boldsymbol{I} - \boldsymbol{K}_k \boldsymbol{H}_k\right) \boldsymbol{P}_{k|k-1} \end{aligned} \tag{7.5}$$

where:

$$\boldsymbol{F}_k = \left.\frac{\partial f}{\partial \boldsymbol{x}}\right|_{\hat{\boldsymbol{x}}_{k-1|k-1}, \boldsymbol{u}_k} \quad \text{and} \quad \boldsymbol{H}_k = \left.\frac{\partial h}{\partial \boldsymbol{x}}\right|_{\hat{\boldsymbol{x}}_{k|k-1}} \tag{7.6}$$

According to (Bernelli) it is possible to write the state space and the system dynamics as:

$$\hat{\boldsymbol{x}}_{k|k-1} = \begin{bmatrix} q(t) \\ \omega(t) \end{bmatrix} \tag{7.7}$$

$$\boldsymbol{F}_k = e^{\boldsymbol{F}\Delta t} \approx (\boldsymbol{I} + \boldsymbol{F}\Delta t) \tag{7.8}$$

where:

$$\boldsymbol{F} = \begin{bmatrix} \boldsymbol{F_{11}} & \boldsymbol{F_{12}} \\ \boldsymbol{0} & \boldsymbol{F_{22}} \end{bmatrix} \tag{7.9}$$

$$\begin{aligned} \boldsymbol{F_{11}} &= \tfrac{1}{2}\begin{bmatrix} 0 & \omega_z & -\omega_y & \omega_x \\ -\omega_z & 0 & \omega_x & \omega_y \\ -\omega_y & -\omega_x & 0 & \omega_z \\ -\omega_x & -\omega_y & -\omega_z & 0 \end{bmatrix} \quad \boldsymbol{F_{12}} = \tfrac{1}{2}\begin{bmatrix} q_4 & -q_3 & q_2 \\ q_3 & q_4 & -q_1 \\ -q_2 & q_1 & q_4 \\ -q_1 & -q_2 & -q_3 \end{bmatrix} \\ \boldsymbol{F_{22}} &= \begin{bmatrix} 0 & \frac{(I_y-I_z)\omega_z}{I_x} & \frac{(I_y-I_z)\omega_y}{I_x} \\ \frac{(I_z-I_x)\omega_z}{I_y} & 0 & \frac{(I_z-I_x)\omega_x}{I_y} \\ \frac{(I_x-I_y)\omega_y}{I_z} & \frac{(I_x-I_y)\omega_x}{I_z} & 0 \end{bmatrix} \end{aligned} \tag{7.10}$$

Equation 7.8 has been recovered thanks to the linearization of the dynamics.
The available measurements are the ones of the Earth Horizon sensor $\boldsymbol{E}$ and the ones of the sun sensor $\boldsymbol{S}$ when possible.

$$\begin{aligned} \boldsymbol{H}_k &= \left.\frac{\partial h(x)}{\partial x}\right|_{x=\hat{x}_{k|k-1}} \quad , \quad H_k = \begin{bmatrix} \boldsymbol{H}_E \\ \boldsymbol{H}_S \end{bmatrix}_{x=\hat{x}_{k|k-1}} \\ \boldsymbol{H}_E &= \frac{\partial \boldsymbol{E}}{\partial x} = \begin{bmatrix} \frac{\partial \boldsymbol{A}}{\partial q_1}\boldsymbol{E} & \frac{\partial \boldsymbol{A}}{\partial q_2}\boldsymbol{E} & \frac{\partial \boldsymbol{A}}{\partial q_3}\boldsymbol{E} & \frac{\partial \boldsymbol{A}}{\partial q_4}\boldsymbol{E} & [\boldsymbol{0}_{3\times 3}] \end{bmatrix} \\ \boldsymbol{H}_S &= \frac{\partial \boldsymbol{S}}{\partial x} = \begin{bmatrix} \frac{\partial \boldsymbol{A}}{\partial q_1}\boldsymbol{S} & \frac{\partial \boldsymbol{A}}{\partial q_2}\boldsymbol{S} & \frac{\partial \boldsymbol{A}}{\partial q_3}\boldsymbol{S} & \frac{\partial \boldsymbol{A}}{\partial q_4}\boldsymbol{S} & [\boldsymbol{0}_{3\times 3}] \end{bmatrix} \\ \frac{\partial \boldsymbol{A}}{\partial q_1} &= 2\begin{bmatrix} q_1 & q_2 & q_3 \\ q_2 & -q_1 & q_4 \\ q_3 & -q_4 & -q_1 \end{bmatrix} \frac{\partial \boldsymbol{A}}{\partial q_2} = 2\begin{bmatrix} -q_2 & q_1 & -q_4 \\ q_1 & q_2 & q_3 \\ q_4 & q_3 & -q_2 \end{bmatrix} \\ \frac{\partial \boldsymbol{A}}{\partial q_3} &= 2\begin{bmatrix} -q_3 & q_4 & q_1 \\ -q_4 & -q_3 & q_2 \\ q_1 & q_2 & q_3 \end{bmatrix} \frac{\partial \boldsymbol{A}}{\partial q_3} = 2\begin{bmatrix} q_4 & q_3 & -q_2 \\ -q_3 & q_4 & q_1 \\ q_2 & -q_1 & q_4 \end{bmatrix} \end{aligned} \tag{7.11}$$

In the Simulink model the Extended Kalman Filter can require too much time for the simulation (3h for the whole orbit). A delay in the filter make the algorithm much faster but leads to instabilities when sun sensors are cut off.

In addition the step function related to the eclipse has been damped with a transfer function of $\frac{1}{s+1}$, otherwise it created problems during the switching between the two phases.

## 7.3 Results

The choice to apply the EKF is due to the angular velocity noisy results with the TRIAD method as the comparison below shows.

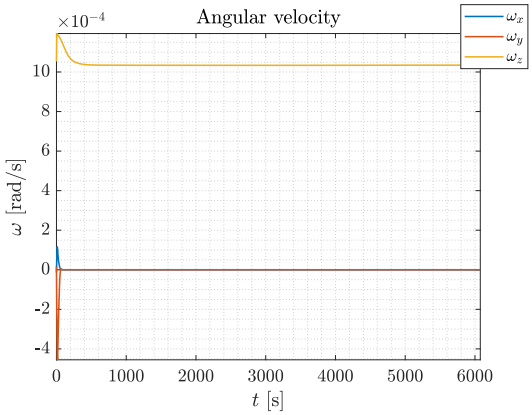


Figure 7.2: Angular velocity with EKF

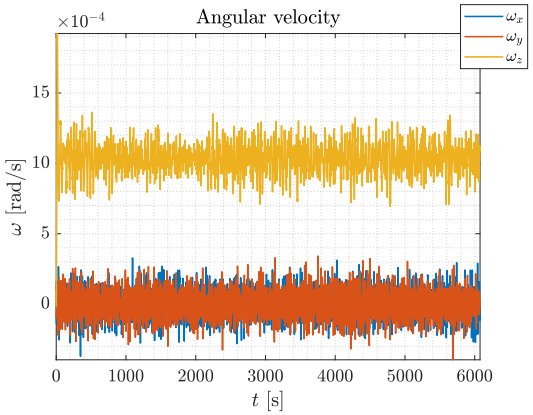


Figure 7.3: Angular velocity without EKF

In this case estimation works much better than determination leading to errors in the order of $< 10^{-5}$ for quaternions and $< 10^{-4}$ $[°/s]$ for angular velocities as displayed in Figure 7.4 and Figure 7.5 respectively. Highest inaccuracies are in the first phase when the switch occurs but then the spacecraft is well aligned for the whole orbit.

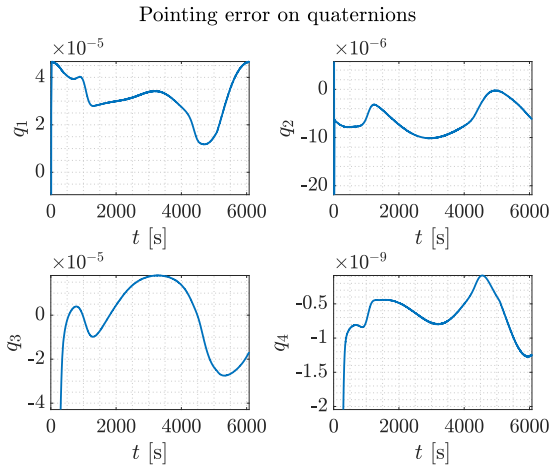


Figure 7.4: Earth pointing accuracy

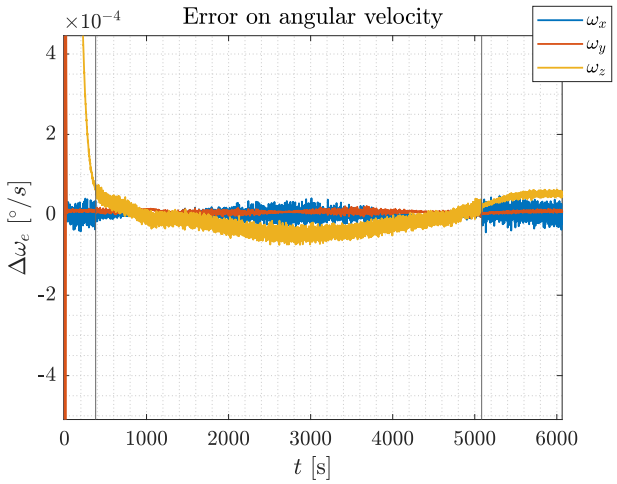


Figure 7.5: Earth pointing error on angular velocities. Vertical lines represent the exit and the enter in the eclipse phase respectively

Good performances of the desired orientation has been also proven by the perfect qualitative match between $A_{ln}$ and $A_{bn}$ shown in Figure 7.6.

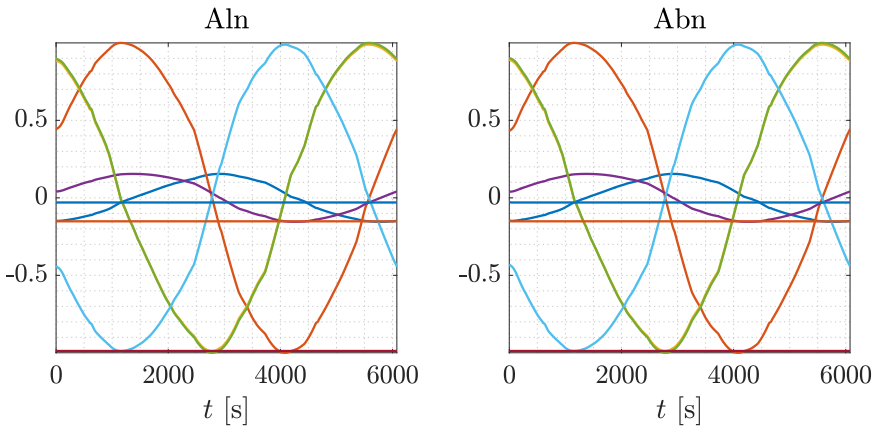


Figure 7.6: Satellite orientation

All the perturbations have been considered in the propagation however only magnetic field and SRP whose torque is of the same order, $10^{-7}$, have been displayed in Figure 7.7. They are also useful to prove the right modelling since the torque is the same at the beginning and at the end of the orbit.

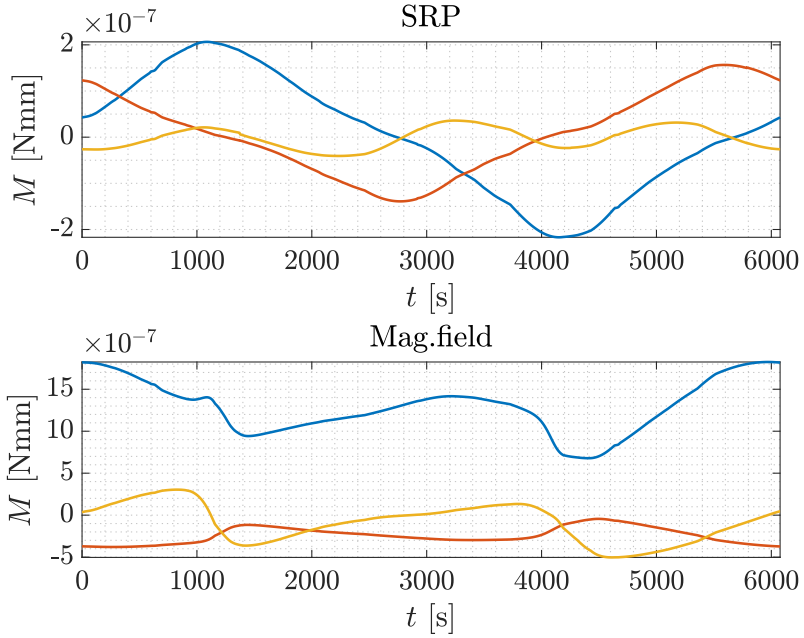


Figure 7.7: Most relevant perturbations during Earth pointing for 1 orbit propagation

# Bibliography

[Bernelli] Bernelli. *Attitude determination and Control System for Palamede Microsatellite.* [Accessed: 24.02.2021]. 20

[Biggs] Biggs. *Lecture notes Prof. Biggs.* [Accessed: 01.01.2021]. 9

[3] IGRF (2020). `https://www.ngdc.noaa.gov/IAGA/vmod/igrf.html`. [Accessed: 03.01.2021]. 10

[MIT] MIT. *Attitude determination for small satellites with infra red Earth Horizon Sensor.* [Accessed: 07.01.2021]. 5